PAPER

Check for updates

Study on thermal behavior and kinetics of Al/MnO₂ poly(vinylidene fluorine) energetic nanocomposite assembled by electrospray

Jiaxing Song,[a] Tao Guo, [iD] *[a] Wen Ding,[a] Miao Yao,[a] Fengli Bei,[b] Xiaonan Zhang,[a] Junyi Huang[a] and Xiang Fang[a]

To explore the effect of the addition of poly(vinylidene fluorine) (PVDF) to a nanothermite system, an Al/MnO₂/PVDF energetic nanocomposite was prepared using an electrospray method, Al/MnO₂ nanothermite was prepared as a control group. Then, the energetic nanocomposite and nanothermite were tested and analyzed by XRD, FE-SEM and TG-DSC, and the reaction products were collected. The results show that energetic nanocomposite would have three obvious exothermic peaks in the range of room temperature to 800 °C with a total more than 1700 J g⁻¹ heat release while the control experiment, Al/MnO₂ nanothermite, could be found one exothermic peak with a 1100 J g⁻¹ heat release. The residues are mainly MnAl₂O₄, MnF₂ and AlF₃ which indicates that Al/MnO₂/PVDF energetic nanocomposite could make full use of manganese oxide. Finally, thermal analysis experiments were carried out under different heating rates to calculate the activation energy. The calculation results show that the addition of PVDF could significantly reduce the activation energy, which would help spark the thermite at comparatively low energy and temperature.

1 Introduction

Nanothermite, as a famous energetic nanocomposite, usually consists of a fuel, an oxidizer and a binder.[1] As for fuel selection, although powdered magnesium is easy to ignite with bright flame, it is dangerous to use nano-scale powdered magnesium in practice due to its spontaneous combustion in the sunshine, even without any open fire.[2,3] On the other hand, the volumetric heat of combustion of aluminum powder is much higher than that of magnesium powder.[4] Therefore, nano-Al is more widely used in energetic nanocomposites than nano-Mg.

However, there is a dense oxide layer, alumina, on the surface of Al powder, which could strongly hinder heat transfer and combustion process. Thus, some researchers have focused on the methods for avoiding or treating the alumina layer. For example, in order to avoid the formation of alumina layer, Kim had reported that nano-Al could be deposited directly onto the CuO nanowires by using RF sputtering under special conditions to prepare the nanocomposite. Through this method, CuO nanowires were coated with nano-Al with more intimate contact and fewer oxidations.[5] Besides, according to some reports about nano-Al/fluoropolymer composites, the reaction of nanoenergetic composites yields aluminum fluoride (AlF₃) which has a much lower boiling point (1276 °C) compared to alumina (about 3000

°C). So some researchers think that AlF₃ might volatilize and hence not hinder the redox reaction between remaining nano-Al and oxidizers.[6] Namely, some fluoropolymers added into nanothermite system as a kind of additive may be a good method to deal with the adverse impact of the alumina layer. In addition, fluorine is the most electronegative element, making it a candidate as an oxidizer in a redox reaction,[7,8] which could improve the combustion characteristic of energetic materials. Zhou[9] has reported that Mg/fluoropolymers core/shell nanoenergetic arrays exhibited a very low onset reaction temperature of about 270 °C with much high heat release, at the same time, the speed of combustion was rapid according to the preliminary combustion test. Besides, the adding of fluoropolymers could bring some other superior properties, for example, anti-humidity and superhydrophobic property.[10,11] Two major fluoropolymers have been used widely, Viton fluoroelastomer (Viton)[12] and polyvinylidene (PVDF).[13] Due to Viton's poor solubility, it is hard to widely use in nanothermite system even though it has the highest content of fluorine in fluoropolymers.[8] Alternatively, PVDF has much great solubility in polar organic solvent, dimethylformamide (DMF).[6] It is formed by vinylidene difluoride, which is widely used in various fields of chemical engineering,[14] and it contains 59.4% fluorine by mass as an oxidizer in some extent and/or reactive binder.[15,16]

According to previous reports,[17,18] Al/MnO₂ thermite system has an adiabatic reaction temperature (calculating phase transition) as high as 2918 K, which is higher than that of Al/CuO thermite, and the amount of gaseous products of Al/MnO₂ thermite system is much higher. As we all know, gaseous products are significant output in highly energetic system,[19]

[a]College of Field Engineering, Army Engineering University of PLA, Nanjing, 210007, China. E-mail: guotao3579@126.com

[b]School of Chemical, Nanjing University of Science and Technology, Nanjing, 210094, China

especially in propellant application. Namely, Al/MnO$_2$ thermite system could be potential energetic materials in the future. Zhu[20] has prepared the 3-D core/shell nanoenergetic arrays of MnO$_2$/Al/fluorocarbon *via* magnetron sputtering based on Si substrate, which showed a superior competence of energy storage.

In this work, we chose PVDF as both oxidizer and reactive binder in the Al/MnO$_2$ nanothermite system. At the same time, in order to prepare much more homogeneous nanothermite, an electrospray method was employed. The precursor was carried forward through a nozzle, and high electric fields were introduced to the gap between the nozzle and receiver. Because of high electrostatic field forces, the Taylor cone is formed at the end of the liquid outflow tube, and in electrospray, the precursor liquid could be broken into plentiful tiny droplets, since the electrostatic force is greater than the molecular cohesive force of the liquid.[21,22] This phenomenon is based on the fact that there is a limit to the number of charges on the surface energy of through droplet.[23,24] Most importantly, the polymer solution used may contain a dispersion of nanoparticles, which remain within the droplets as the precursor jet undergoes break up. The solvent in the fine charged droplets rapidly evaporate as they are extracted and accelerated by the extracting electric field, leaving concentrated nanoparticles and polymer, which were finally collected onto a substrate to create a uniform, high nanoparticle loading polymer composite.[25] To explore the effect of the addition of poly(vinylidene fluorine) (PVDF) in nanothermite system, Al/MnO$_2$ nanothermite was also prepared as a control group. Then, the Al/MnO$_2$/PVDF nanocomposite and Al/MnO$_2$ nanothermite were tested and analyzed by XRD, FE-SEM and TG-DSC. According to the results of TG-DSC at different heating rate, the kinetics of both samples were calculated and discussed. The addition of PVDF in thermite could great reduce the activation energy, which would help spark the thermite at comparatively low energy and temperature. It is helpful for their further application.

2 Experimental

2.1 Materials

All chemicals were analytical reagent grade and were used without any further treatment or purification. KMnO$_4$ and HCl were used for MnO$_2$ nanorods synthesis, which were supplied by Lingfeng Chemical Reagent Co., LTD. (Shanghai, China). The Al nanoparticles with 100 nm average diameter were purchased from Aladdin Industrial Corporation (Shanghai, China). Polyvinylidene (PVDF), as an energetic additive, was supplied by Sinopharm Chemical Reagent Co., Ltd. In addition, the absolute ethanol and dimethylformamide (DMF) were supplied by Nanjing Chemical Reagent Co., Ltd, and absolute ethanol, DMF as well as deionized water were selected as solvent and dispersant.

2.2 Synthesis of nano-MnO$_2$

Nano-MnO$_2$ was synthesized *via* hydrothermal method as following: 3 g KMnO$_4$ was dissolved into 20 mL deionized water, which was stirred intensely by using the magnetic stirring apparatus for about 20 min. Next, 1.875 mL HCl was extracted

by pipette and diluted with 10 mL deionized water. Then, the diluted HCl solution was added dropwise into the stirring KMnO$_4$ solution. After that, the mixture solution was transferred into a 50 mL Teflon-lined stainless steel autoclave, sealed and maintained at 200 °C for 6 h in an electric oven. When the autoclave was cooled to the room temperature, the products were taken out, which was a dark brown granule. The obtained powder was washed for several times with deionized water and ethyl alcohol, respectively. After the centrifugal operation, the product was dried at 80 °C for 12 h.

2.3 Preparation of precursor

At first, nano-MnO$_2$ and Al nanoparticles were weighted based on stoichiometric ratio, and then the mixture of MnO$_2$ and Al were ultrasonicated for about 30 min in ethanol. At the same time, PVDF was dissolved into DMF. In a typical experiment, 40 mg Al nanoparticles and 60 mg nano-MnO$_2$ were dispersed in 3 mL ethanol, and 43 mg PVDF was dissolved in 1 mL DMF solvent (the oxidation layer of Al nanoparticles is taken into consideration). So the mass fraction of PVDF in nanothermite system was about 30 wt%. Then, the PVDF/DMF solution was poured into mixed turbid ethanol under ultrasonic conditions. Besides, Al/MnO$_2$ nanothermite without PVDF additive was also prepared as the control experiment.

2.4 Electrospray experiment

As shown in Fig. 1, a syringe pump was used to eject the precursor fluid with the velocity of 4.0 mL h^{-1}, and thinner diameter of the nozzle at the end was 0.43 mm. In order to form a Taylor cone, 13 kV positive voltage was loaded on the nozzle, and the negative electrode was connected to the receiver plate. The relative humidity during the experiment was about 75%. Under the action of electrostatic field, droplets flied from the nozzle to the receiving plate, and the distance between the nozzle and receiving plate was about 10 cm. In this process, the solvent quickly volatilized and droplets formed solid particles that deposit on the receiving plate (square aluminum foil with the side length of 30 cm). Finally, we gently scraped off the powder deposited on the aluminum foil and collected it into the anti-static vial for later use.

2.5 Characterization analysis

The samples, including synthesized nano-MnO$_2$, PVDF, nanothermite and reaction products, were characterized by using XRD analysis (Bruker, D8 Advance, Germany) and synthesized
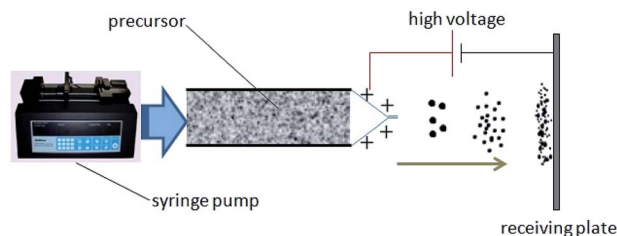

Fig. 1 Schematic diagram of electrospray experiment.

nano-MnO$_2$ were also characterized by using XPS analysis (Escalab 250Xi, USA). The morphologies, particle size and mixing quality of the samples were characterized by FE-SEM analysis (Carl-Zeiss Merlin FE-SEM, Germany; HITACHI High-Technologies Corporation, S-4800 II Japan).

2.6 Thermal analysis

The investigation of thermal behavior was carried out based on the DSC (Mettle-Toledo 1600LF-PTM90611234, USA) analysis. The sample mass was about 3 mg in corundum crucible, covering the temperature range from room temperature to 800 °C in argon atmosphere.

2.7 Theoretical background

In this work, the famous Kissinger method was used in the calculation of thermal kinetics of Al/MnO$_2$ thermite mixtures. The activation energy was calculated through Kissinger method based on the DSC peak temperature.[26,27] This method can be expressed by the following equation:

$$\ln\left(\frac{\beta}{T_p{}^2}\right) = \ln\frac{AR}{E_a} - \frac{E_a}{RT_p} \tag{1}$$

where β is the linear heating rate (°C min^{-1}), and T_p is the absolute temperature of DSC peak temperature (K), and R is the universal gas constant (J mol^{-1} K^{-1}), and A is the pre-exponential factor (s^{-1}) and E_a is the activation energy (kJ mol^{-1}). Thus, the plot of $\ln(\beta/T_p{}^2)$ *versus* $1/T_p$ should be a straight line whose slope can be used to evaluate the activation energy. The degree of credibility will be higher if the absolute value of the correlation coefficient is much closer to 1 theoretically.

3 Results and discussion

3.1 Results of synthesized nano-MnO$_2$

In order to figure out the characteristics of obtained sample by hydrothermal method, both XRD and XPS were introduced to test the phase and valence state while the FE-SEM was used to observe the morphology.

3.1.1 XRD analysis. Fig. 2 presents the XRD patterns of the obtained sample, which corresponds to the tetragonal MnO$_2$
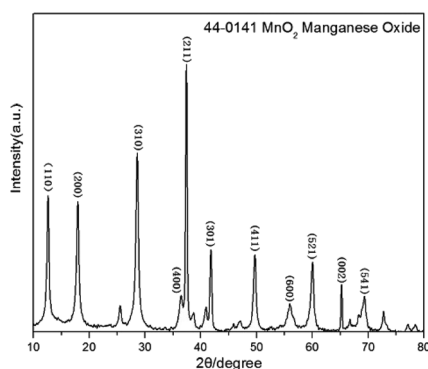
(manganese oxide) phase (ICDD/JCPDS 44-0141 MDI Jade 6.0). The lattice constants are $a = b = 9.785$ Å, $c = 2.863$ Å and space group is $I4/m(87)$. There are no distinct anomalous peaks and the matching degree is good.

3.1.2 XPS analysis. As is known to all, the crystallinity of nanomaterials is usually much poorer comparing to micron-level materials. Therefore, we selected XPS to test the valence state of obtained sample. As shown in Fig. 3(a), it can be easy to find the two most intense peaks in the spectrum, oxygen (O) and manganese (Mn). Due to the raw material KMnO$_4$, there is the certain intensity indicating the potassium (K). Table 1 lists the peak details of XPS spectrum data. Remarkably, in Fig. 3(b) the peak of Mn 2p$_{3/2}$ is about 642.44 eV, which means the valence state of Mn is (4+) based on previous studies,[28,29] and Zhou[30] recently has also reported that the peak at 642.77 eV is consistent with Mn^{4+}. In addition, the energy separation of 11.64 eV between Mn 2p$_{3/2}$ and Mn 2p$_{1/2}$ peaks are consistent with those in MnO$_2$, and there is also another peak energy separation of 4.65 eV is obtained from the high-resolution spectrum of Mn 3s in Fig. 3(c), which is in agreement with the oxidation state of Mn at 4.[20] As for the listing of atomic% in Table 1, the ratio of the content of Mn to O is about 1 : 2.

3.1.3 SEM analysis. Fig. 4 shows the FE-SEM images of synthesized nano-MnO$_2$. Fig. 4(a) is the overall FE-SEM image of synthesized nano-MnO$_2$. For more accurate observation, the red box in Fig. 4(a) is magnified, as shown in Fig. 4(b). The morphology of the sample is nanorod with smooth surface. The diameter of the sample is about a dozen nanometers.
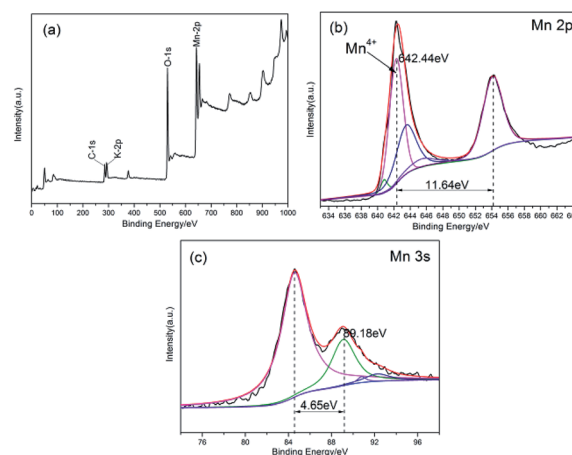

Fig. 3 Survey XPS spectrum of synthesized nano-MnO$_2$. (a) Full XPS spectrum, (b) Mn 2p, (c) Mn 3s.

Table 1 Data details of peak in XPS spectrum^a

Name	Start BE	Peak BE	End BE	Atomic%
C 1s	291.03	284.79	279.98	20.24
K 2p	305.88	292.03	287.98	6.00
O 1s	545.88	529.83	525.98	50.81
Mn 2p	664.88	642.44	632.98	22.95

^{a} BE: abbreviation of binding energy.

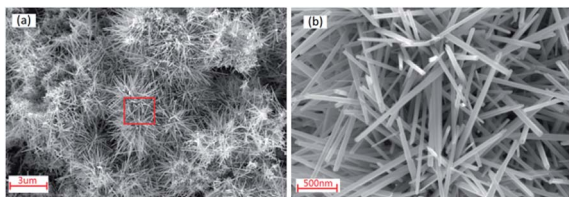**Fig. 2** XRD patterns of synthesized nano-MnO$_2$.

Fig. 4 FE-SEM images of synthesized nano-MnO_2.

3.2 Results of nanocomposite and nanothermite

3.2.1 XRD analysis. Fig. 5 shows the XRD pattern of PVDF and nanocomposite as well as nanothermite. The black line represents the pure PVDF. The blue line is the XRD results of energetic nanocomposites Al/MnO_2/PVDF-30 wt% while the red one is that of the control experiment, Al/MnO_2 nanothermite. Noticeably, it is hard to find any characteristic peak of PVDF in blue line even though it has 30 wt% PVDF in nanocomposites. Namely, as for the blue line, there are merely characteristic peaks of both Al and MnO_2, which is the same as the red line. According to precursor preparation method, both Al powder and MnO_2 powder are directly dispersed into the ethanol, but PVDF is dissolved into the DMF. Under the high voltage electric field, the solvent of precursor evaporates rapidly. As for Al powder and MnO_2 powder, they are directly deposited on the surface receiving plate. As for PVDF/DMF solution, the PVDF should go through a recrystallization process under normal circumstances. However, in this electrospray experiment, it is difficult to recrystal under high voltage electric field, especially for polymers, which leads to the phenomenon that there is no evident characteristic peak of XRD pattern.

3.2.2 SEM analysis. There is no evident characteristic peak of the PVDF in Al/MnO_2/PVDF nanocomposites system, but it is easy to find the PVDF component from FE-SEM images.

Fig. 6 shows the morphologies of nanocomposites. In Fig. 6(a), it is the Al/MnO_2 nanothermite prepared by electrospray. The MnO_2 nanorods and Al nanoparticles are dispersed relatively evenly, and plenty of Al nanoparticles directly adhere to the surface of MnO_2 nanorods with little agglomerations. As is known to all, the phenomenon of nanomaterials agglomerations is universal and unavoidable to some extent.[31]
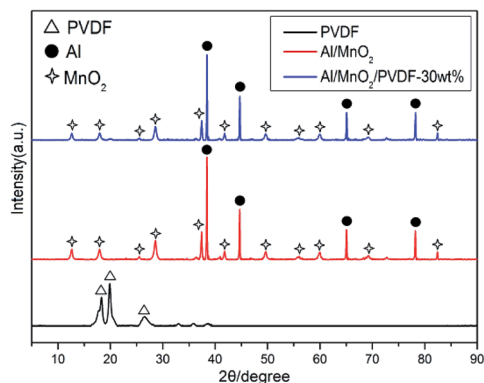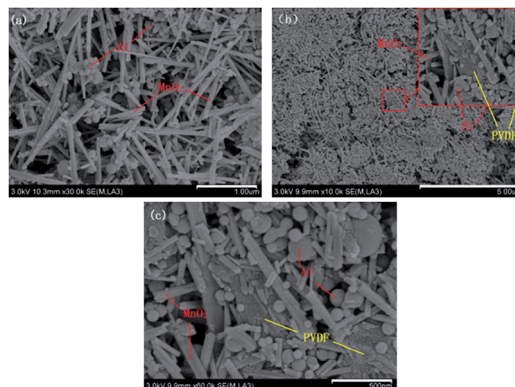

Fig. 6 FE-SEM images of nanocomposites, (a) Al/MnO_2 nanothermite, (b) Al/MnO_2/PVDF nanocomposite, (c) magnified image of Al/MnO_2/PVDF nanocomposite.

Electrospray is one of the useful preparation methods to reduce the impact of agglomerations. Fig. 6(b) shows the nanostructure of Al/MnO_2/PVDF nanocomposite and Fig. 6(c) is the magnified image of Al/MnO_2/PVDF nanocomposite. On the one hand, PVDF, as a kind of binder, could combine Al nanoparticles with MnO_2 nanorods. On the other hand, as a kind of fluorine polymer, when the temperature rises to a certain degree, there is a thermal decomposition process, an exothermic process, which could release fluorine and then participate in the exothermic thermite reaction.[6]

In order to find out the components distribution of Al/MnO_2/PVDF nanocomposite, SEM-mapping is introduced, shown in Fig. 7. Fig. 7(a) shows the chosen SEM-mapping scan area. In Fig. 7(b), (c) and (d), the Mn and Al element are on behalf of the MnO_2 nanorods component and Al nanoparticles, respectively, and the F element is selected as characteristic element of PVDF, shown in Fig. 7(b) and (e). All components are dispersed evenly.

3.3 Thermal analysis and kinetics calculation

3.3.1 TG-DSC analysis. In order to investigate the thermal process and effect of PVDF addition in nanothermite system, the pure PVDF powder, Al/MnO_2 nanothermite and Al/MnO_2/PVDF energetic nanocomposite were characterized by using
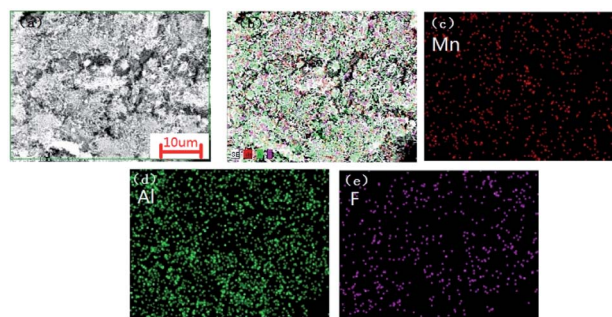

Fig. 5 XRD pattern of the samples.

Fig. 7 SEM-mapping of Al/MnO_2/PVDF nanocomposite, (a) mapping scan area, (b) the general distribution of elements, (c) distribution of Mn element, (d) distribution of Al element, (e) distribution of F element.
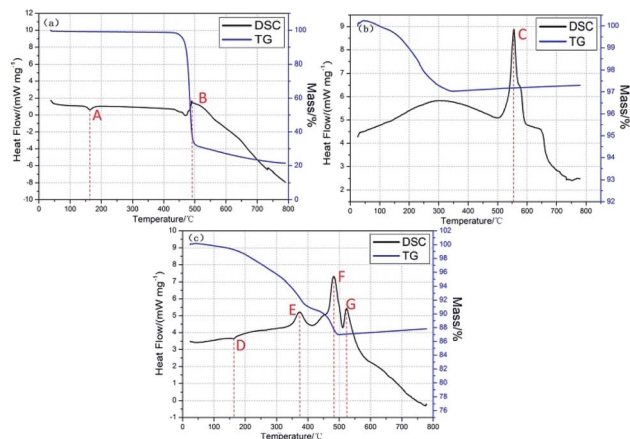
Fig. 8   TG-DSC analysis results (a) TG-DSC curve of PVDF, (b) TG-DSC curve of Al/MnO$_2$ nanothermite, (c) TG-DSC curve of Al/MnO$_2$/PVDF energetic nanocomposite.

Fig. 9   XRD pattern of reaction products.

Fig. 10   DSC curves at different heating rates (a) Al/MnO$_2$ nanothermite, (b) Al/MnO$_2$/PVDF nanocomposite.

thermal analysis experiments, TG-DSC tests. The results are shown in Fig. 8 and the peak temperature of each peak are listed in Table 2. The heating rates of these three experiments are same, 10 °C min^{-1} under the 30 mL min^{-1} argon atmosphere.

In Fig. 8(a), the TG-DSC curve of PVDF, there are two obvious peaks. Peak A, an endothermic peak, represents the melting process of PVDF.[6,32] The melting point is about 160 °C with no mass change in TG curve. When the temperature rises to 450–550 °C, an exothermic peak (Peak B) with about 536.99 J g^{-1} heat release corresponded to a sharp mass loss by TG curve due to the decomposition of PVDF. At the end of experiment, the remaining mass is about 20%.

In Fig. 8(b), the TG-DSC curve of Al/MnO$_2$ nanothermite, there is merely one main peak. Before the temperature reaches 330 °C, there is no significant signal in DSC curve, but the mass of sample continues to decline about −3% because of desorption of both physisorbed and structural H$_2$O and ethanol,[33,34] which is the norm. The main exothermic peak (Peak C) appears at 552.129 °C ahead of the melting point of Al (about 660 °C). The onset temperature of Peak C is about 520 °C and the endset is about 580 °C, with 1137.64 J g^{-1} heat release.

In Fig. 8(c), the TG-DSC curve of Al/MnO$_2$/PVDF energetic nanocomposite, there are four obvious peaks from room temperature to 800 °C, three exothermic peaks (Peak E, F and G) and one endothermic peak (Peak D). Apparently, the endothermic peak (Peak D) is caused by PVDF melting. Before the temperature reaches 330 °C, the reason why there is a continuous mass loss is that water and ethanol are evaporated gradually. Next, TG curve still has a downward tendency with the first exothermic peak appears (Peak E) with 359.16 J g^{-1} heat
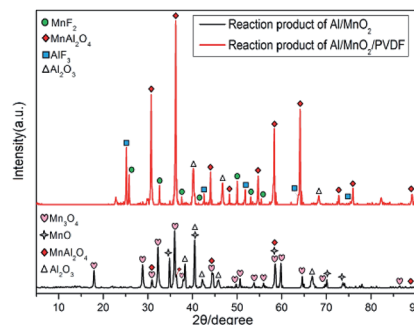
release. According to previous report,[6] the heat release is caused by the reaction between the Al nanoparticles and PVDF polymer matrix. The peak temperature of Peak E is 374.157 °C while the onset and endset temperature are 348.671 °C and 397.67 °C, respectively.

Then, as for TG curve, there is a sharp mass loss in the range of 450 to 500 °C with about 891.45 J g^{-1} heat releases. According to the discussion of Fig. 8(a), it is caused by the thermal decomposition of PVDF and the reaction of Al nanoparticles and PVDF degradation products. Besides, the thermite reaction could be sparked partly. Namely, we guess that there are several possible reactions in Peak F, the decomposition of PVDF, the reaction between Al nanoparticles and PVDF degradation products, the thermite reaction as well as the reaction between MnO$_2$ nanorods and PVDF degradation products. The peak temperature of Peak F is 482.96 °C while the onset and endset temperature are 463.58 °C and 508.79 °C, respectively.

In the end, as for Peak G, it should be the thermite reaction between Al nanoparticles and MnO$_2$ nanorods with about 476.81 J g^{-1} heat releases, and there is no obvious mass change in TG curve, indicating oxygen transfer from the MnO$_2$ to the Al. Due to the addition of PVDF, the thermite reaction is sparked early, comparing to Fig. 8(b). Besides, all of the above reactions

Table 2   Details of each peak in TG-DSC curves

No.	Type	Peak temperature	No.	Type	Peak temperature
A	Endothermic	163.295 °C	B	Exothermic	490.022 °C
C	Exothermic	552.129 °C	D	Endothermic	161.785 °C
E	Exothermic	374.157 °C	F	Exothermic	482.964 °C
G	Exothermic	523.830 °C			

Table 3 Details of peak temperature at different heating rates

Reactant		Heating rates and corresponding peak temperature			
		10 K min^{-1}	15 K min^{-1}	20 K min^{-1}	Average
Al/MnO$_2$ nanothermite		552.13 °C (825.28 K)	555.64 °C (828.79 K)	559.02 °C (832.17 K)	555.60 °C (828.75 K)
Al/MnO$_2$/PVDF nanocomposite	A area	373.31 °C (646.46 K)	376.23 °C (649.38 K)	384.37 °C (657.52 K)	377.97 °C (651.12 K)
	B area	482.96 °C (756.11 K)	489.72 °C (762.87 K)	493.30 °C (766.45 K)	488.66 °C (761.81 K)
	C area	523.32 °C (796.47 K)	528.69 °C (801.84 K)	533.74 °C (806.89 K)	528.58 °C (801.73 K)

processes happen below the melting point of Al, which means the state of Al is still in solid phase.

3.3.2 Reaction products analysis. In order to fully understand the thermal process, the reaction products are collected and analyzed by XRD tests, as shown in Fig. 9. The black line is the XRD pattern of the reaction product of Al/MnO$_2$ nanothermite while the red one is that of Al/MnO$_2$/PVDF nanocomposite. PVDF, as a kind of energetic additive, could provide the strongest oxidizing element, F element, and according to the results of TG-DSC analysis as well as the reaction products XRD pattern, it will directly affect the reaction processes and results.

In Fig. 9, the main reaction products of Al/MnO2 nanothermite are Mn$_3$O$_4$, MnO, MnAl$_2$O$_4$ and Al$_2$O$_3$ from the black line. Comparatively, the main reaction products of Al/MnO$_2$/PVDF nanocomposite are MnF$_2$, MnAl$_2$O$_4$, AlF$_3$ and Al$_2$O$_3$ from the red line. There is no evidence about the presence of any kind of manganese oxide, neither Mn$_3$O$_4$ nor MnO, not to mention MnO$_2$. Namely, all of manganese oxide are involved into reaction and are fully utilized, which could release much more heat and energy. To some extent, the addition of PVDF will prompt the exothermic reaction to take place more fully.

3.3.3 Kinetics analysis. Activation energy can be used to represent the minimum energy required for a chemical reaction to occur. The activation energy can reflect the degree of difficulty of chemical reaction. The reaction of Al/MnO$_2$ thermite is usually difficulty to spark, which is one of the reasons that

seriously restrict its wide application. To some extent, lowering the activation energy could promote the initiation of the thermite reaction. At the argon atmosphere, the DSC tests are carried out at different heating rates, 10 K min^{-1}, 15 K min^{-1} and 20 K min^{-1}. In Fig. 10, both two samples have the similar thermal processes at different heating rates.

The famous Kissinger method is chosen to calculate the activation energy of Al/MnO$_2$ nanothermite and Al/MnO$_2$/PVDF nanocomposite. We chose the three main exothermic peaks from DSC curves (A, B and C areas) which could represent the whole reaction, and the details of each peak temperature at different heating rates are listed in Table 3. According to the theoretical background, the Celsius degree should be converted to Kelvin degree. Based upon the Kissinger method mentioned in eqn (1), the plots of $\ln(\beta/T_p^2)$ *vs.* $1/T_p$ at the peak temperature are constructed in Fig. 11. Fig. 11(a) shows the result of Al/MnO$_2$ nanothermite, and the analytical expression of the data correlation line is $y = -66188x + 70.018$. The correlation coefficient R is about -0.9888, and the activation energy E_a, deduced from the slope of the data correlation line, is about 550.29 kJ mol^{-1}. In the same way, as for the result of Al/MnO$_2$/PVDF nanocomposite in Fig. 11(b), (c) and (d), the analytical expression of the data correlation lines are $y = -23634x + 26.004$, $y = -36763x + 37.656$, $y = -41218x + 40.708$, respectively, and the correlation coefficient R are about -0.9501, -0.9964 and -0.9968, respectively. Thus, in contrast, the activation energy E_a, deduced from the slope of the data correlation lines, are about 196.49 kJ mol^{-1}, 305.65 kJ mol^{-1} and 342.68 kJ mol^{-1}. Usually, when the thermite is ignited successfully, it can maintain combustion without external energy input, which is called self-propagation. Namely, after the main exothermic reaction, the thermite reaction should start, which means that the reaction no longer requires external energy. So, the activation energy of C area is meaningless to some extent. Here, we pay much attention to the activation energy of the main exothermic reaction (B area). The activation energy is significantly reduced by about 244.64 kJ mol^{-1} due to the addition of PVDF.

4 Conclusions

In this work, the MnO$_2$ nanorods are synthesized successfully *via* hydrothermal method and characterized firstly. Then the Al/MnO$_2$/PVDF energetic nanocomposite is prepared by electrospray method, and Al/MnO$_2$ nanothermite is also prepared by the same way as the control group. Electrospray method can effectively reduce agglomerations of nanomaterials. According
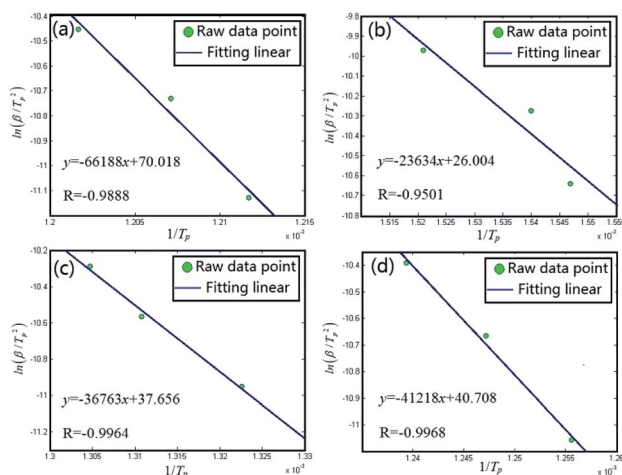

Fig. 11 The data correlation line according to Kissinger method (a) Al/MnO$_2$ nanothermite, (b) A area of Al/MnO$_2$/PVDF nanocomposite, (c) B area of Al/MnO$_2$/PVDF nanocomposite, (d) C area of Al/MnO$_2$/PVDF nanocomposite.

to the results of TG-DSC analysis, $Al/MnO_2/PVDF$ energetic nanocomposite will have three obvious exothermic peaks in the range of room temperature to 800 °C with total more than 1700 J g^{-1} heat releases while the control experiment, Al/MnO_2 nanothermite, could be found one exothermic peak with about 1100 J g^{-1} heat releases, which means that PVDF as a kind of energetic additive could significantly improve the thermal properties of thermite system. As for reaction products, the residues of $Al/MnO_2/PVDF$ energetic nanocomposite are mainly $MnAl_2O_4$, MnF_2 and AlF_3, indicating that $Al/MnO_2/PVDF$ energetic nanocomposite could make full use of manganese oxide. In contrast, the residues of the control group have a certain mass of manganese oxide. In the end, thermal analysis experiments are carried out under different heating rates to calculate the activation energy by using the Kissinger method. The results show that the addition of PVDF not only improves the thermal performance, but also significantly reduces the activation energy, which would help spark the thermite at comparatively low energy and temperature.

Conflicts of interest

The authors declare that there is no conflict of interest regarding the publication of this paper.

Acknowledgements

Notes and references

1 M. L. Pantoya, V. I. Levitas, J. J. Granier, et al., Effect of Bulk Density on Reaction Propagation in Nanothermites and Micron Thermites, J. Propul. Power, 2009, 25, 465.

2 S. G. Hosseini, A. Sheikhpour, M. H. Keshavarz and S. Tavangar, The effect of metal oxide particle size on the thermal behavior and ignition kinetic of Mg-CuO thermite mixture, Thermochim. Acta, 2016, 626, 1.

3 L. Liu, H. Ren and Q. J. Jiao, Effect of Nano-Magnesium on the Thermal Decomposition of PTFE, Mater. Sci. Forum, 2014, 809, 155.

4 L. H. Shen, L. I. Guoping, Y. J. Luo, K. Gao and Z. Ge, Preparation and characterization of $Al/B/Fe_2O_3$ nanothermites, Science, 2014, 57, 797.

5 D. K. Kim, J. H. Bae, M. K. Kang and H. J. Kim, Analysis on thermite reactions of CuO nanowires and nanopowders coated with Al, Curr. Appl. Phys., 2011, 11, 1067.

6 C. Huang, H. Yang, Y. Li and Y. Cheng, Characterization of Aluminum/Poly(Vinylidene Fluoride) by Thermogravimetric Analysis, Differential Scanning Calorimetry, and Mass Spectrometry, Anal. Lett., 2015, 48, 2011.

7 K. W. Watson, M. L. Pantoya and V. I. Levitas, Fast reactions with nano- and micrometer aluminum: a study on oxidation versus fluorination, Combust. Flame, 2008, 155, 619.

8 X. Hu, J. B. Delisio, X. Li, et al., Direct Deposit of Highly Reactive $Bi(IO_3)_3$-Polyvinylidene Fluoride Biocidal Energetic Composite and its Reactive Properties, Adv. Eng. Mater., 2017, 19, 1.

9 X. Zhou, D. Xu, G. Yang, et al., Highly Exothermic and Superhydrophobic Mg/Fluorocarbon Core/Shell Nanoenergetic Arrays, ACS Appl. Mater. Interfaces, 2014, 6, 10497.

10 X. Zhou, Y. Zhu, K. Zhang, et al., An extremely superhydrophobic and intrinsically stable Si/fluorocarbon energetic composite based on upright nano/submicron-sized Si wire arrays, RSC Adv., 2015, 5, 106098.

11 X. Zhou, D. Xu, J. Lu and K. Zhang, CuO/Mg/fluorocarbon sandwich-structure superhydrophobic nanoenergetic composite with anti-humidity property, Chem. Eng. J., 2015, 266, 163–170.

12 R. H. B. Bouma, D. Meuken, R. Verbeek, M. M. Pacheco and L. Katgerman, Shear initiation of Al/MoO_3-based reactive materials, Propellants, Explos. Pyrotech., 2007, 32, 447.

13 K. Meeks, M. L. Pantoya and C. Apblett, Deposition and characterization of energetic thin film, Combust. Flame, 2014, 161, 1117.

14 Y. Wang, J. T. Sejdic and R. Steiner, Polymer gel electrolyte supported with microporous polyolefin membranes for lithium ion polymer battery, Solid State Ionics, 2002, 148, 443.

15 H. A. Miller, B. S. Kusel, S. T. Danielson, et al., Metastable nanostructured metallized fluoropolymer composites for energetics, J. Mater. Chem. A, 2013, 1, 7050.

16 Q. L. Yan, S. Zeman and A. Elbeih, Thermal behavior and decomposition kinetics of Viton A bonded explosives containing attractive cyclic nitramines, Thermochim. Acta, 2013, 562, 56.

17 N. H. Yen and L. Y. Wang, Reactive metals in explosives, Propellants, Explos., Pyrotech., 2012, 37, 143.

18 S. Elbasuney, Novel Colloidal Nanothermite Particles (MnO2/Al) for Advanced Highly Energetic Systems, J. Inorg. Organomet. Polym. Mater., 2018, 28, 1793.

19 P. P. Vadhe, R. B. Pawar, R. K. Sinha, et al., Cast aluminized explosives (review), Combust., Explos. Shock Waves, 2008, 44, 461.

20 Y. Zhu, X. Zhou, C. Wu, H. Cheng, et al., Si Wire Supported MnO2/Al/Fluorocarbon 3D Core/Shell Nanoenergetic Arrays with Long-Term Storage Stability, Sci. Rep., 2017, 7, 6678.

21 X. Yuan and S. V. Hoa, Mechanical properties of carbon fiber reinforced epoxy/clay nanocomposites, Compos. Sci. Technol., 2008, 68, 854.

22 G. V. Kumar, C. Rao and N. Selvaraj, Mechanical and dry sliding wear behavior of Al7075 alloy-reinforced with SiC particles, J. Compos. Mater., 2012, 46, 1201.

23 A. Jaworek, Micro- and nanoparticle production by electrospraying, Powder Technol., 2007, 176, 18.

24 N. Bock, M. A. Woodruff, D. W. Hutmacher, et al., Electrospraying, a reproducible method for production of

polymeric microspheres for biomedical applications, *Polymers*, 2011, **3**, 131.

25 X. Li and M. R. Zachariah, Direct Deposit of Fiber Reinforced Energetic Nanocomposites, *Propellants, Explos. Pyrotech.*, 2017, **42**, 1.

26 H. E. Kissinger, Reaction Kinetics in Differential Thermal Analysis, *Anal. Chem.*, 1957, **29**, 1702.

27 P. E. Sánchez-Jiménez, J. M. Criado and L. A. Pérez-Maqueda, Kissinger kinetic analysis of data obtained under different heating schedules, *J. Therm. Anal. Calorim.*, 2008, **94**, 427.

28 V. A. M. Brabers, F. M. van Setten and P. S. A. Knapen, X-ray photoelectron spectroscopy study of the cation valencies in nickel manganite, *J. Solid State Chem.*, 1983, **49**, 93.

29 J. C. Carver, G. K. Schweitzer and T. A. Carlson, Use of X-ray photoelectron spectroscopy to study bonding in Cr, Mn, Fe, and Co compounds, *J. Chem. Phys.*, 1972, **57**, 973.

30 J. Zhou, L. Cao, Q. Wang, *et al.*, Enhanced Hg^0 removal *via* α-MnO_2 anchored to MIL-96(Al), *Appl. Surf. Sci.*, 2019, DOI: 10.1016/j.apsusc.2019.03.261.

31 A. Singhal, G. Skandan, A. Wang, *et al.*, On nanoparticle aggregation during vapor phase synthesis, *Nanostruct. Mater.*, 1999, **11**, 545.

32 S. F. Mendes, C. M. Costa, V. Sencadas, *et al.*, Thermal degradation of $Pb(Zr_{0.53}Ti_{0.47})O_3$/poly(vinylidene-fluoride) composites as a function of ceramic grain size and concentration, *J. Therm. Anal. Calorim.*, 2013, **114**, 757.

33 R. A. Williams, M. Schoenitz, A. Ermoline, *et al.*, Low-temperature exothermic reactions in fully-dense Al/MoO3 nanocomposite powders, *Thermochim. Acta*, 2014, **594**, 1.

34 W. M. Dose and S. W. Donne, Manganese dioxide structural effects on its thermal decomposition, *Mater. Sci. Eng., B*, 2011, **176**, 1169.